Observing the Nonequilibrium Dynamics of the Quantum Transverse-Field Ising Chain in Circuit QED

Oliver Viehmann,[1] Jan von Delft,[1] and Florian Marquardt[2]

[1]*Physics Department, Arnold Sommerfeld Center for Theoretical Physics, and Center for NanoScience,
Ludwig-Maximilians-Universität, Theresienstraße 37, 80333 München, Germany*
[2]*Institut for Theoretical Physics, Universität Erlangen-Nürnberg, Staudtstraße 7, 91058 Erlangen, Germany*
(Received 9 August 2012; published 15 January 2013)

We show how a quantum Ising spin chain in a time-dependent transverse magnetic field can be simulated and experimentally probed in the framework of circuit QED with current technology. The proposed setup provides a new platform for observing the nonequilibrium dynamics of interacting many-body systems. We calculate its spectrum to offer a guideline for its initial experimental characterization. We demonstrate that quench dynamics and the propagation of localized excitations can be observed with the proposed setup and discuss further possible applications and modifications of this circuit QED quantum simulator.

The promising idea of tackling complex quantum many-body problems by quantum simulations [1,2] has become even more compelling recently, due to the widespread current interest in nonequilibrium dynamics. Indeed, experiments with cold atoms in optical lattices [3–6] and ions [7–10] have already made impressive progress in this regard. At the same time, the capabilities of scalable, flexible solid-state platforms are developing rapidly. In particular, circuit quantum electrodynamics (cQED) architectures of superconducting artificial atoms and microwave resonators [11–19] are now moving toward multiatom, multiresonator setups with drastically enhanced coherence times, making them increasingly attractive candidates for quantum simulations [20]. Here, we propose and analyze a cQED design that simulates a quantum transverse-field Ising chain with current technology. Our setup can be used to study quench dynamics, the propagation of localized excitations, and other nonequilibrium features in a field theory exhibiting a quantum phase transition (QPT) [21] and based on a design that could easily be extended to break the integrability of the system.

The present Letter takes a different path than the proposals for simulating Bose-Hubbard-type many-body physics in cavity arrays, which might be also realizable in cQED [20,22–26]. It is based on a possibly simpler concept—direct coupling of artificial atoms—that naturally offers access to quantum magnetism. The transverse-field Ising chain (TFIC) is a paradigmatic quantum many-body system. It is exactly solvable [27,28] and thus serves as a standard theoretical example in the context of nonequilibrium thermodynamics and quantum criticality [21,29–34]. Our proposal to simulate the TFIC and its nonequilibrium dynamics might help to mitigate the lack of experimental systems for testing these results. Moreover, the experimental confirmation of our predictions for various nonequilibrium scenarios in this integrable many-body system would

serve as an important benchmark and allow one to proceed to variations of the design that break integrability or introduce other features.

Implementation of the TFIC.—A charge-based artificial atom (such as the Cooper-pair box or the transmon) [35] in a superconducting microwave resonator can be understood as an electric dipole (with dipole operator σ_x) that couples to the quantized electromagnetic field in the resonator [36]. Consider the system of Fig. 1, at first, without resonator *B*. Only the first artificial atom couples to resonator *A*. However, all atoms couple directly (not mediated by a quantized field) to their neighbors via dipole-dipole coupling $\propto \sigma_x^i \sigma_x^j$ (for details, see Ref. [37]). Coupling of this type has already been demonstrated with two Cooper-pair boxes [38] and two transmons [19]. Since this interaction is short ranged, we model our system by

$$\mathcal{H} = \omega_0(a^\dagger a + 1/2) + g(a^\dagger + a)\sigma_x^1 + \mathcal{H}_I, \quad (1)$$

where $\mathcal{H}_I$ is the Hamiltonian of the TFIC,

$$\mathcal{H}_I = \frac{\Omega}{2} \sum_{j=1}^{N} \sigma_z^j - J \sum_{j=1}^{N-1} \sigma_x^j \sigma_x^{j+1}. \quad (2)$$
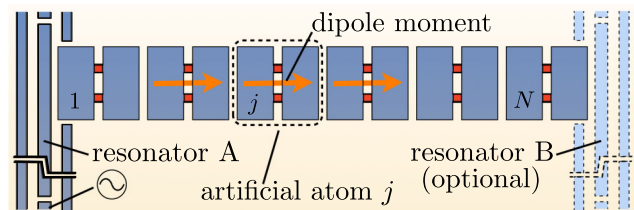
FIG. 1 (color online). Circuit QED implementation of the Ising model with a transverse magnetic field. The dipole moments of the artificial atoms tend to align. Resonator *A* (*B*) facilitates initialization and readout of the first (*N*th) artificial atom by standard circuit QED techniques.

Here, $a^\dagger$ generates a photon with frequency ω_0, and $\sigma_{x/z}^j$ is a Pauli matrix. That is, we consider the artificial atoms as two-level systems (qubits). This is justified even for weakly anharmonic transmons since the experiments proposed below involve only low atomic excitation probabilities or well controllable excitation techniques (π pulses). Qubit 1 and the resonator couple with strength g. The qubit level spacing $\Omega > 0$ is tunable rapidly (~ 1 ns) via the magnetic flux through the qubits' SQUID loops [11–14]. It corresponds to the transverse magnetic field in the usual TFIC. In our geometry, the qubit-qubit coupling strength J is positive (ferromagnetic; the antiferromagnetic coupling $J < 0$ arises by rotating each qubit in Fig. 1 by 90° and is discussed in Ref. [37]). Estimates based on the typical dimensions of a cQED system yield $J/2\pi \sim 100$ MHz. Interdigitated capacitors between the qubits might significantly increase J. In general, tuning Ω will also affect J in a way that depends on the tuning mechanism and on the fundamental qubit parameters [37]. Using standard technology, upon variation of the magnetic flux, $J \propto \Omega$ for transmons, whereas, for Cooper-pair boxes, J is independent of Ω. Resonator A facilitates the initialization and readout of qubit 1 (with standard techniques [11]). Resonator B would allow one to measure end-to-end correlators. However, for simplicity, we consider a system with one resonator unless otherwise noted. We mention that the proposed setup should also be implementable using the novel, high-coherence 3d cQED devices [39]. Superconducting flux and phase qubits [35] can also be coupled to implement $\mathcal{H}_I$ and related Hamiltonians [15,17]. For different proposals on the implementation of and mean-field-type experiments with the TFIC in cQED, see Refs. [40,41], respectively.

In our calculations [37], we frequently use the spin-free-fermion mapping for $\mathcal{H}_I$ from Refs. [27,28]. It yields $\mathcal{H}_I = \sum_k \Lambda_k(\eta_k^\dagger \eta_k - 1/2)$, where $\eta_k^\dagger$ generates a fermion of energy $\Lambda_k = 2J\sqrt{1 + \xi^2 - 2\xi \cos k}$ and $\xi = \Omega/2J$ is the normalized transverse field. The allowed values of k satisfy $\sin kN = \xi \sin k(N+1)$. For $N \to \infty$, $\mathcal{H}_I$ undergoes the second order QPT at $\xi = 1$ from a ferromagnetic phase ($\xi < 1$) with long-range order in σ_x to a disordered, paramagnetic phase (for details, see Refs. [21,27,28,37]).

Spectrum of the system.—An initial experiment would likely characterize the setup by measuring the transmission spectrum S of the resonator as a function of probe frequency ω and qubit frequency Ω. For definiteness, we now assume that J is fixed and that the transverse field $\xi = \Omega/2J$ is tunable via Ω, as is the case for Cooper-pair boxes. A system with standard transmons can be shown to be confined to the paramagnetic phase (with fixed $\xi > 1$), but its spectrum as a function of ω and $J \propto \Omega$ otherwise displays the same features [37]. To calculate S, we first focus on the spectrum of the bare TFIC, $\tilde{\rho}(\omega) = \int dt\, e^{i\omega t} \langle \sigma_x^1(t)\sigma_x^1(0)\rangle$. It shows at which frequencies a field coupled to σ_x^1 can excite the chain. Assuming $g/\omega_0 \ll 1$,

we then approximate the chain as a linear bath, coupled to the resonator: We replace it by a set of harmonic oscillators with the spectrum $\tilde{\rho}(\omega)$ of the TFIC. This allows us to compute S. Our calculations are for zero temperature. Except near the QPT, where $\mathcal{H}_I$ becomes gapless, this is experimentally well justified.

For finite N, the calculated spectrum $\tilde{\rho}(\omega)$ would consist of discrete peaks. In an experiment, they would be broadened by decay and, for large N, the measured spectrum would be continuous. This can be modeled by taking $N \to \infty$ in our calculations. In that case,

$$\tilde{\rho}(\omega) = 2\pi\delta(\omega)\Theta(1-\xi)(1-\xi^2) + \frac{4\xi}{\omega}\mathrm{Re}\sqrt{1 - \cos^2 k(\omega)} \tag{3}$$

for $\omega \gtrsim 0$, and $\tilde{\rho}(\omega < 0) = 0$. Here, $\Theta(x)$ is the Heaviside step function, and $\cos k(\omega) = [1 + \xi^2 - (\frac{\omega}{2J})^2]/2\xi$. The delta function for $\xi < 1$ is due to the nonzero mean value of $\mathrm{Re}\langle \sigma_x^1(t)\sigma_x^1(0)\rangle$ in this phase. We plot $\tilde{\rho}(\omega)$ for several ξ in Fig. 2(a). For $\xi > 1$ ($\xi < 1$), $\tilde{\rho}$ has a width of $4J$ ($4J\xi$), the bandwidth of the Λ_k. This might be helpful to measure J. At $\xi = 1$, $\tilde{\rho}$ becomes gapless and, thus, carries a clear signature of the QPT. The loss of normalization for $\xi = 0.5$ is compensated by the delta function in (3). This is required by a sum rule for $\tilde{\rho}$ and can be understood: In the ordered phase, the ground state $|0\rangle$ of the TFIC becomes similar to a σ_x eigenstate. Thus, driving via σ_x^1 is less efficient in causing excitations out of $|0\rangle$, but a static force on σ_x^1 will change the energy of $|0\rangle$. We note that, for all ξ, $\tilde{\rho}(\omega)$ has its maximum where the band Λ_k has zero curvature (and maximum slope). Thus, most η_k excitations
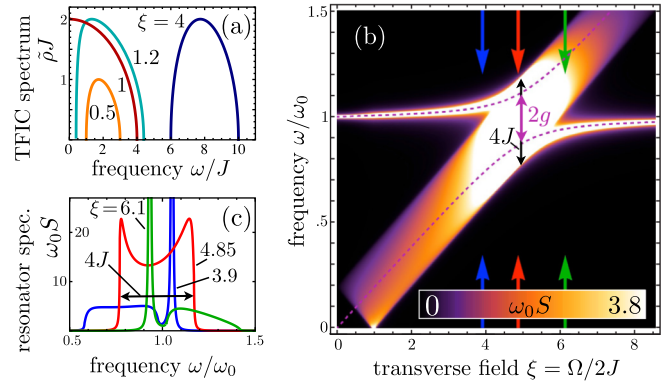
FIG. 2 (color online). Spectrum of the system. (a) Spectrum $\tilde{\rho}(\omega) = \int dt\, e^{i\omega t}\langle\sigma_x^1(t)\sigma_x^1(0)\rangle$ of an isolated transverse-field Ising chain for $N \to \infty$ and normalized transverse fields $\xi = \Omega/2J = 4, 1.2, 1, 0.5$. (b) Spectrum S of a resonator coupled to a TFIC (as in Fig. 1), plotted vs ξ and ω (for $N \to \infty$). The parameters used are $g = 0.12$, $J = 0.1$, and $\kappa = 10^{-4}$ (in units of ω_0). For better visibility of the features, values >3.8 are plotted in white. The dashed lines represent the excitation energies of $\mathcal{H}$ for $N = 1$. (c) S vs ω for $\xi = 3.9, 4.85, 6.1$ (blue, red, and green lines, respectively). These lines correspond to cuts along the arrows in (b).

of the TFIC have a nearly uniform velocity $v_0 = \max[d\Lambda_k/dk]$ ($v_0 = 2J\xi$ for $\xi < 1$ and $v_0 = 2J$ for $\xi > 1$), which will be important below.

We obtain resonator spectrum $S(\omega)$ in terms of $\tilde{\rho}(\omega)$,

$$S(\omega) = \frac{4\Theta(\omega)[\kappa + g^2\tilde{\rho}(\omega)]}{[\omega^2/\omega_0 - \omega_0 - 4g^2\chi(\omega^2)]^2 + [\kappa + g^2\tilde{\rho}(\omega)]^2}. \tag{4}$$

Here, $\chi(\omega^2)$ denotes the principal value integral $\chi(\omega^2) = 1/(2\pi)\int d\Omega\,\tilde{\rho}(\Omega)\Omega/(\omega^2 - \Omega^2)$ and κ is the full linewidth at half maximum of the Lorentzian spectrum of the uncoupled ($g = 0$) resonator. Our calculation uses tools that are explained, e.g., in Ref. [42]. It actually also applies when the resonator couples to a different system, with another spectrum $\tilde{\rho}(\omega)$. We plot S as function of ω and ξ in Fig. 2(b). For comparison, we also plot the resonances of the Jaynes-Cummings model, as they have been observed in numerous cQED experiments (dashed lines; case $N = 1$ in $\mathcal{H}$). As long as the spectrum $\tilde{\rho}(\omega)$ of the chain does not overlap the resonator frequency ω_0, there is a dispersive shift analogous to the off-resonant single-qubit case. Here, the chain causes only a small but broad side maximum and hardly modifies the dominant Lorentzian [green and blue lines in Fig. 2(c)]. If the chain comes into resonance, this changes dramatically, and $S(\omega)$ takes on large values over a region of width $\sim 4J$. For our choice of parameters, $S(\omega)$ develops a slightly asymmetric double-peak structure [red line in Fig. 2(c)]. This is again reminiscent of the Jaynes-Cummings doublet, but now the peaks are split by $4J$ rather than $2g$. We emphasize that the shape of the spectrum on resonance depends significantly on the ratio g/J. The larger $g/J > 1$, the closer the system resembles the single-qubit case (corresponds to $J = 0$). If $g/J < 1$, the double peak vanishes and one observes a Lorentzian around ω_0 with width $2g^2/J$ (for $g^2/J \gg \kappa$). This is because the resonator irreversibly decays into the chain, whose inverse bandwidth $\propto 1/J$ sets the density of states at $\omega \approx \omega_0$ and so determines the decay rate (for plots on both limiting cases and for finite N, see Ref. [37]).

Propagation of a localized excitation.—Off resonance, chain and resonator are essentially decoupled. In this situation, our setup allows one to study nonequilibrium dynamics in the TFIC. The resonator can be used to dispersively read out the first qubit. For measurements, this qubit must be detuned (faster than $2\pi/J$ from the chain so that it dominates the dispersive shift of the resonator [11] and decouples from the chain's dynamics.

First, we focus on the nonequilibrium dynamics of the chain after a local excitation has been created. As the resonator couples only to one qubit, the initialization of the system is easy. We assume that the chain is far in the paramagnetic phase ($\xi \gg 1$). Hence, $\langle\sigma_z^j\rangle \approx -1$ in its ground state. By applying a fast (~ 1 ns) π pulse, the first spin of the chain can be flipped without affecting the state of the other qubits (if $J/2\pi \ll 1$ GHz$/2\pi$ or if the first

qubit is detuned from the others for initialization). We model the state of the system immediately after the π pulse by $\sigma_x^1|0\rangle$, where $|0\rangle$ is the ground state of the TFIC. The time evolution of the qubit excitations $\langle\sigma_z^j\rangle$,

$$\langle\sigma_z^j\rangle(t) = \langle 0|\sigma_x^1 e^{i\mathcal{H}_I t}\sigma_z^j e^{-i\mathcal{H}_I t}\sigma_x^1|0\rangle, \tag{5}$$

is plotted in Fig. 3 for a chain with $N = 20$ and $\xi = 8$ (right panel). The experimentally measurable trace of $\langle\sigma_z^1\rangle(t)$ is singled out on the left-hand side. Due to the qubit-qubit coupling, the excitation propagates through the chain, is reflected at its end, and leads to a distinct revival of $\langle\sigma_z^1\rangle$ at $Jt_R \approx N$. Assuming $J/2\pi = 50$ MHz, we find $t_R \approx 64$ ns for $N = 20$, which is safely below transmon coherence times. Note that the excitation propagates with velocity $v_0 = 2J$. This is because it consists of many excitations in k space, and most of them have velocity v_0.

Quench dynamics.—An appealing application of our system would be to observe its nonequilibrium dynamics after a sudden change of the transverse field $\xi = \Omega/2J$. By using fast flux lines, changes of Ω have been achieved practically instantaneously on the dynamical time scale of a cQED system (without changing the wave function) [12–14]. In our setup, such a change amounts to a (global) quantum quench of ξ if $J \not\equiv \Omega$. This condition can be fulfilled by using qubits whose Josephson and charging energies [35] have a ratio $E_J/E_C \lesssim 10$ [37], that is, Cooper-pair boxes or transmons slightly out of their optimal parameter ratio [43]. In this regime, the tuning of J with Ω is weak (vanishes for Cooper-pair boxes). Since it would only lead to a rescaling of time by a factor ~ 1, we assume in the following that J is independent of Ω and consider quantum quenches of ξ in our system. Quantum quenches in the TFIC have been studied theoretically, e.g., in Refs. [30–33]. One usually assumes that for $t < 0$ the system is in the ground state $|0\rangle_a$ of the Hamiltonian $\mathcal{H}_{I,a}$
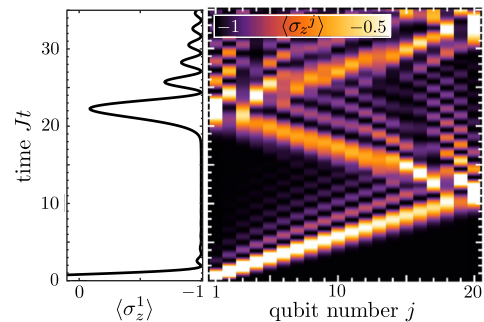
FIG. 3 (color online). Propagation of a localized excitation. Right: nonequilibrium time evolution of $\langle\sigma_z^j\rangle$ for all qubits j of a transverse Ising chain of length $N = 20$ in a normalized transverse field $\xi = \Omega/2J = 8$ (paramagnetic phase) after the first spin has been flipped. Values > -0.5 are plotted in white. Left: separate plot of $\langle\sigma_z^1\rangle$ on the same time scale. This quantity can be measured in the setup of Fig. 1.

at some initial value $\xi_a = \Omega_a/2J$. At $t = 0$, ξ is changed to $\xi_b = \Omega_b/2J$, and the time evolution under the action of $\mathcal{H}_{I,b}$ is investigated.

In the following, we focus on the dynamics of the experimentally easily accessible observable $\langle\sigma_z^1\rangle$ after quenches within the paramagnetic phase. This corresponds to our estimates for realistic values of J. The main difference of quenches involving the ferromagnetic phase would be a modified dynamical time scale due to the different value of v_0. Figure 4 shows the magnetization $\langle\sigma_z^j\rangle(t)$ after quenching ξ (center). In region I (see schematic plot, right), the magnetization first increases and then oscillates with decreasing amplitude. Here, it is virtually identical with the overall magnetization of a cyclic TFIC with $N \to \infty$ calculated in Ref. [30] and would, for $N \to \infty$, approach a constant value. This is in line with predictions from conformal field theory [32]. However, at $t = j/v_0$ and $t = (N - j)/v_0$ (dashed red lines in the schematic plot), where $v_0 = 2J$ as before, the magnetization has dips. They are followed (in regions II and III) by a relaxation similar as in region I to the same asymptotic value (see Ref. [37] for a zoomed-in plot). Near the system boundaries, the magnetization reaches and stays at this value for a considerable time before undergoing a revival. A sharp oscillation across the entire chain at $T = N/v_0$ subsequently decays. Revivals reoccur (quasi-)periodically with period T (region IV), but this behavior is smeared out for large times (not plotted). These phenomena are reflected in the measurable observable $\langle\sigma_z^1\rangle(t)$ (left panel) and take place on a time scale of ~ 0.1 μs for $N = 30$ and $J/2\pi = 50$ MHz.

Our results can be qualitatively understood in a simplifying quasiparticle (QP) picture that has already been used to calculate or interpret the (quench) dynamics of different quantities in the TFIC [31–34]. In the paramagnetic phase, the QPs correspond to spins pointing in the $+z$ direction. They are created in pairs by the quench and ballistically move with velocities $\pm v_0$ with reflections at the
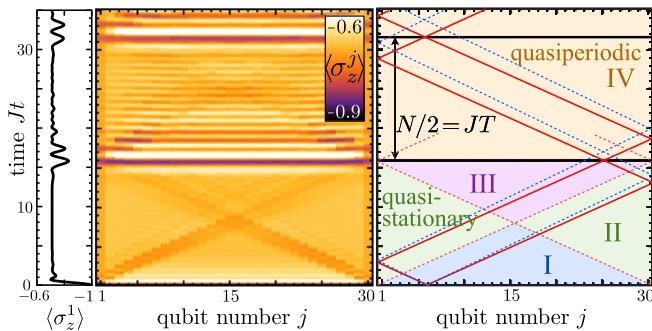
boundaries. Further, only contiguously generated QPs are correlated. After an initial transient, any given site will be visited only by uncorrelated QPs, originating from distant places. This leads to the relaxation of the magnetization to a steady-state value in region I that would be characterized by a certain static density of uncorrelated QPs. However, once correlated QPs meet again due to reflections at the boundaries, coherences are recreated and show up in oscillation revivals. This happens, first, at multiples of T (black solid lines in the schematic plot) when all QP trajectories cross their momentum-inverted counterparts (the solid red lines show an example) and, second, along the trajectories of QP pairs generated at the boundaries. Such QPs travel together as one partner is reflected at $t \approx 0$ (dashed red lines, not plotted in region IV for clarity). The periodicity of the trajectories should lead to periodic revivals for $t > T$. This is indeed observed approximately, although finally the velocity dispersion of the QPs renders the time evolution quasiperiodic. Finally, QP trajectories cannot intersect at $j = 1$, N. The density of (incoherent) QPs is thus lower here than for bulk sites, yielding an appreciably lower quasistationary value.

Discussion and outlook.—The setup and the experiments we have proposed might help to establish the simulation of interacting quantum many-body systems as a new paradigm in circuit QED and to bring parts of the theoretical discourse in nonequilibrium physics closer to observation. The phenomena discussed here are based on realizable system parameters and should occur within the system's coherence time. Given the readout capabilities in cQED (e.g., Ref. [16]), their measurement should be feasible, for instance, because single-shot readout is not required. Once an actual implementation sets some boundary conditions, the choice of system parameters can be further optimized. We have numerically verified that all presented results are robust against disorder up to a few percent in Ω and J [44]. Detuning individual qubits, however, would allow one to create arbitrary potentials for the excitations, study the interplay of Anderson localization and many-body physics, or change the effective chain length. Using a second resonator, the dynamics of the end-to-end correlator $\langle\sigma_x^1\sigma_x^N\rangle$ (indicating long-range order) could be measured (see Ref. [37]). Many other experiments are conceivable with our setup, such as suddenly coupling two isolated chains (and other local quenches) or even parameter ramps through the QPT, with Kibble-Zurek defect creation. We note also that hitherto unexplored measurement physics could be studied when the first qubit is not detuned from the chain, like resolving many-body eigenstates or the quantum Zeno effect in a many-body system. Once the setup is properly understood, it will be easy to break the integrability of our model in a controlled way (e.g., via longer-range couplings). This would push our cQED quantum simulator into a regime beyond classical computational capabilities, where further open questions about nonequilibrium

FIG. 4 (color online).   Behavior after a quench: time evolution of the magnetization $\langle\sigma_z^j\rangle$ in a TFIC of length $N = 30$ after a quench of the normalized transverse field $\xi = 8 \to 1.2$ (center) with a schematic plot (right) and the measurable observable $\langle\sigma_z^1\rangle$ singled out (left) on the same time scale. Values < -0.9 (> -0.6) are plotted in black (white).

dynamics can be addressed, such as thermalization and diffusive transport. Furthermore, going to 2d or 3d introduces new design options, for instance, frustrated lattices.

[1] R. Feynman, Int. J. Theor. Phys. **21**, 467 (1982).

[2] I. Buluta and F. Nori, Science **326**, 108 (2009).

[3] D. Jaksch, C. Bruder, J. I. Cirac, C. W. Gardiner, and P. Zoller, Phys. Rev. Lett. **81**, 3108 (1998).

[4] M. Greiner, O. Mandel, T. Esslinger, T. W. Hänsch, and I. Bloch, Nature (London) **415**, 39 (2002).

[5] J. Simon, W. S. Bakr, R. Ma, M. E. Tai, P. M. Preiss, and M. Greiner, Nature (London) **472**, 307 (2011).

[6] S. Trotzky, Y.-A. Chen, A. Flesch, I. P. McCulloch, U. Schollwöck, J. Eisert, and I. Bloch, Nat. Phys. **8**, 325 (2012).

[7] A. Friedenauer, H. Schmitz, J. T. Glueckert, D. Porras, and T. Schaetz, Nat. Phys. **4**, 757 (2008).

[8] R. Islam et al., Nat. Commun. **2**, 377 (2011).

[9] B. P. Lanyon, C. Hempel, D. Nigg, M. Muller, R. Gerritsma, F. Zahringer, P. Schindler, J. T. Barreiro, M. Rambach, G. Kirchmair, M. Hennrich, P. Zoller, R. Blatt, and C. F. Roos, Science **334**, 57 (2011).

[10] J. W. Britton, B. C. Sawyer, A. C. Keith, C.-C. J. Wang, J. K. Freericks, H. Uys, M. J. Biercuk, and J. J. Bollinger, Nature (London) **484**, 489 (2012).

[11] A. Wallraff, D. I. Schuster, A. Blais, L. Frunzio, R.-S. Huang, J. Majer, S. Kumar, S. M. Girvin, and R. J. Schoelkopf, Nature (London) **431**, 162 (2004).

[12] L. DiCarlo, M. D. Reed, L. Sun, B. R. Johnson, J. M. Chow, J. M. Gambetta, L. Frunzio, S. M. Girvin, M. H. Devoret, and R. J. Schoelkopf, Nature (London) **467**, 574 (2010).

[13] A. Fedorov, L. Steffen, M. Baur, M. P. da Silva, and A. Wallraff, Nature (London) **481**, 170 (2012).

[14] M. D. Reed, L. DiCarlo, S. E. Nigg, L. Sun, L. Frunzio, S. M. Girvin, and R. J. Schoelkopf, Nature (London) **482**, 382 (2012).

[15] R. McDermott, R. W. Simmonds, M. Steffen, K. B. Cooper, K. Cicak, K. D. Osborn, S. Oh, D. P. Pappas, J. M. Martinis, Science **307**, 1299 (2005).

[16] R. Vijay, D. H. Slichter, and I. Siddiqi, Phys. Rev. Lett. **106**, 110502 (2011).

[17] M. W. Johnson et al., Nature (London) **473**, 194 (2011).

[18] M. Mariantoni et al., Science **334**, 61 (2011).

[19] A. Dewes, F. Ong, V. Schmitt, R. Lauro, N. Boulant, P. Bertet, D. Vion, and D. Esteve, Phys. Rev. Lett. **108**, 057002 (2012).

[20] A. A. Houck, H. E. Türeci, and J. Koch, Nat. Phys. **8**, 292 (2012).

[21] S. Sachdev, Quantum Phase Transitions (Cambridge University Press, Cambridge, England, 1999).

[22] M. J. Hartmann, F. G. S. L. Brandao, and M. B. Plenio, Nat. Phys. **2**, 849 (2006).

[23] A. D. Greentree, C. Tahan, J. H. Cole, and L. C. L. Hollenberg, Nat. Phys. **2**, 856 (2006).

[24] J. Koch and K. L. Hur, Phys. Rev. A **80**, 023811 (2009).

[25] M. Schiró, M. Bordyuh, B. Öztop, and H. E. Türeci, Phys. Rev. Lett. **109**, 053601 (2012).

[26] M.-J. Hwang and M.-S. Choi, arXiv:1207.0088.

[27] E. Lieb, T. Schultz, and D. Mattis, Ann. Phys. (N.Y.) **16**, 407 (1961).

[28] P. Pfeuty, Ann. Phys. (N.Y.) **57**, 79 (1970).

[29] A. Polkovnikov, K. Sengupta, A. Silva, and M. Vengalattore, Rev. Mod. Phys. **83**, 863 (2011).

[30] E. Barouch, B. McCoy, and M. Dresden, Phys. Rev. A **2**, 1075 (1970).

[31] F. Iglói and H. Rieger, Phys. Rev. Lett. **85**, 3233 (2000).

[32] P. Calabrese and J. Cardy, Phys. Rev. Lett. **96**, 136801 (2006); J. Stat. Mech. (2007) P06008.

[33] H. Rieger and F. Iglói, Phys. Rev. Lett. **106**, 035701 (2011); Phys. Rev. B **84**, 165117 (2011).

[34] S. Sachdev and A. P. Young, Phys. Rev. Lett. **78**, 2220 (1997).

[35] J. Clarke and F. Wilhelm, Nature (London) **453**, 1031 (2008).

[36] R. J. Schoelkopf and S. M. Girvin, Nature (London) **451**, 664 (2008).

[37] See Supplemental Material at http://link.aps.org/supplemental/10.1103/PhysRevLett.110.030601 for our explicit calculations and some additional details.

[38] Yu. A. Pashkin, T. Yamamoto, O. Astafiev, Y. Nakamura, D. V. Averin, and J. S. Tsai, Nature (London) **421**, 823 (2003).

[39] H. Paik et al., Phys. Rev. Lett. **107**, 240501 (2011).

[40] Y.-D. Wang, F. Xue, Z. Song, and C.-P. Sun, Phys. Rev. B **76**, 174519 (2007).

[41] L. Tian, Phys. Rev. Lett. **105**, 167001 (2010).

[42] F. Marquardt and D. S. Golubev, Phys. Rev. A **72**, 022113 (2005).

[43] J. Koch, T. Yu, J. Gambetta, A. Houck, D. Schuster, J. Majer, A. Blais, M. Devoret, S. Girvin, and R. Schoelkopf, Phys. Rev. A **76**, 042319 (2007).

[44] O. Viehmann, J. von Delft, and F. Marquardt (to be published).